Inhibition of KDM5A/B promotes antitumor innate immune responses in HHV-8/KSHV-positive B-cell lymphomas

Authors:

Dawei Zhou[1], Guillaume N Fiches[1], Zhenyu Wu[1], Suha Eleya[1], Youngmin Park[1], Jinshan He[1], Kateepe ASN Shanaka[1], Thurbu T Lepcha[1], Yan Liu[1], Jason Oliva[2], Kathryn Lurain[3], Jae U Jung[4], Jun Qi[5], Weiqiang J Zhao[1], Jian Zhu[1,*], Netty G Santoso[1,*]

Affiliations:

1. Department of Pathology, College of Medicine, The Ohio State University, Columbus, OH 43210, USA

2. Department of Molecular Genetics, College of Arts and Science, The Ohio State University, Columbus, OH 43210, USA

3. Division of Hematology, Department of Internal Medicine, College of Medicine, The Ohio State University, Columbus, OH 43210, USA

4. Department of Microbial Sciences in Health, and Global Center for Pathogen and Human Health Research, Cleveland Clinic Research, Cleveland Clinic, Cleveland, OH 44195, USA

5. Department of Cancer Biology, Dana-Farber Cancer Institute, Boston, MA, 02215, USA

*To whom correspondence should be addressed: Jian Zhu (Jian.Zhu@osumc.edu) or Netty Santoso (Netty.Santoso@osumc.edu)

Key words: KDM5, KSHV, lytic reactivation, viral oncolysis, antitumor immunity, lymphoma

Summary/Abstract

Histone methylation is a dynamic and reversible epigenetic modification that critically controls the progression of human diseases, including infections and cancers. Here we reported that histone lysine demethylases (KDMs) in the KDM5 family KDM5A/B play profound roles in suppressing lytic reactivation of oncogenic human herpesvirus 8 (HHV-8), i.e., Kaposi's sarcoma-associated herpesvirus (KSHV), as well as antiviral/antitumor innate immune responses in KSHV-infected B-cell lymphomas. We showed that KSHV lytic replication decreases KDM5A/B protein stability by enhancing their K-48 linked polyubiquitination while KDM5A/B depletion facilitates KSHV lytic reactivation. Mechanistic studies illustrated that KDM5A/B associate with KSHV LANA protein and dampen its chromatin association at both KSHV viral lytic promoter and promoters of antitumor immune-responsive genes (IRGs). In comparisons to normal B cells, KDM5A/B expression significantly increased in B-cell lymphoma cells, including KSHV-positive primary effusion lymphoma (PEL). We demonstrated that KDM5A/B inhibition remarkably induces both KSHV lytic reactivation and innate immune responses in PEL cells, resulting in a strong viral oncolytic effect, both *in vitro* in cell cultures and *in vivo* using a PEL xenograft mouse model. Overall, our studies identified the novel functions of KDM5A/B to silence KSHV lytic replication and antiviral/antitumor innate immune responses, which can be blocked to benefit the treatment of KSHV-associated B-cell lymphomas that are usually aggressive and difficult to treat.

47

48 **Introduction**

49 HHV-8/KSHV is a human gamma-herpesvirus and an etiological agent of multiple
50 malignancies, including Kaposi's sarcoma(1), primary effusion lymphoma (PEL)(2), and
51 multicentric Castleman's disease (CAD)(3). Once KSHV enters the host cells, it goes through
52 brief lytic replication and establishes latent infection by maintaining viral genomes as extra-
53 chromosomal circular episomes in nuclei with most viral lytic genes silenced(4,5). KSHV lytic
54 reactivation can be triggered by certain stimuli so that new progeny viruses are generated for
55 viral propagation(6). Such latent/lytic switch of KSHV is delicately controlled by both viral and
56 host regulators, including KSHV-encoded latency-associated nuclear antigen (LANA) and
57 replication and transcription activator (RTA) proteins, host transcription and epigenetic factors,
58 and host factors that participate in immune responses(7). KSHV latent/persistent infection is
59 known to promote cell survival, proliferation and immune evasion, eventually leading to tumor
60 initiation and progression(8). On the other hand, it has been tempted to induce KSHV lytic
61 reactivation in KSHV-positive tumor cells so that viral oncolysis effect is achieved(9).
62 Therefore, it is critical to elucidate profound KSHV-host interactions, especially epigenetic
63 regulatory mechanisms that govern viral latent/lytic switch and persistent infection, which will
64 benefit the therapeutic development for treating KSHV-associated malignancies.

65 Earlier studies have revealed the functional relevance of epigenetic regulation, including
66 histone methylation/demethylation modifications, in KSHV-host interactions(10-13). However,
67 only limited host factors participating in these epigenetic processes have been characterized,
68 which have primarily focused on those targeting histone methylation sites that associate with
69 transcriptional inactivation, such as H3K9 and H3K27. On the contrary, it has been barely

70 examined regarding the contributions of histone methylation sites that associate with
71 transcriptional activation (H3K4, H3K36) as well as modification enzymes targeting these sites
72 to KSHV viral infection and/or KSHV-induced tumorigenesis. The KDM5 family members
73 (KDM5A-D) are capable of removing methyl groups from the tri- and di-methylation of lysine 4
74 of histone H3 (H3K4me3/me2) that usually peak at the promoter regions of actively transcribed
75 genes, which generally results in gene suppression phenotype(14). In particular, KDM5A and
76 KDM5B (KDM5A/B) are ubiquitously expressed and play a critical role in controlling cell
77 proliferation and differentiation. There is strong evidence that KDM5A/B are oncogenes
78 overexpressed, amplified, or mutated in multiple types of human cancers(15). Based on the
79 continuous efforts of our earlier KDM5A/B studies(16-18), we demonstrated that KSHV lytic
80 program targets KDM5A/B for proteasome degradation while KDM5A/B suppresses KSHV
81 lytic reactivation and antiviral/antitumor innate immune responses in KSHV-positive B-cell
82 lymphomas, which can be inhibited to induce viral oncolysis effect *in vitro* and *in vivo*.
83
84 **Results**
85 **KSHV lytic program targets KDM5A/B for proteasome degradation.** An early proteomic
86 study has implicated that KSHV lytic replication may lead to the reduction of host proteins(17).
87 We first evaluated whether KSHV impacts KDM5 proteins. We relied on the PEL cell line
88 BCBL-1 harboring the latently infected KSHV genome while also carrying an integrated cassette
89 for doxycycline (Dox) induced RTA expression (TREx.BCBL-1.RTA). Dox treatment potently
90 reactivated latent KSHV in TREx.BCBL-1.RTA cells (**Fig S1A**), which indeed dramatically
91 reduced the protein level of KDM5A/B (**Fig 1A**) and KDM5C (**Fig S1B**). In contrast, their
92 mRNA levels were not significantly affected (**Fig 1B, S1C**). Dox treatment had no such effects

93 on the BJAB cells, a KSHV-negative Burkitt lymphoma (BL) cell line (**Fig 1C, 1D, S1D, S1E**).
94 We further determined KSHV's impact on KDM5 proteins during its *de novo* infection. The
95 telomerase-immortalized human endothelial (TIME) cells were spinoculated with KSHV BAC16
96 viruses (**Fig S1F, S1G**), which also dramatically decreased the protein level of KDM5A/B (**Fig**
97 **1E**) and KDM5C (**Fig S1H**) while only slightly reducing their mRNA level (**Fig 1F, S1I**).
98 Based on these results, we hypothesized that KDM5 protein stability is affected by KSHV
99 lytic program. To prove this, we treated the TREx.BCBL-1.RTA cells with a proteasome
100 inhibitor MG132 (+/− Dox). MG132 restored the KDM5A/B protein level that was reduced due
101 to Dox treatment (**Fig 1G**). Consistently, we showed that the K48-linked polyubiquitination of
102 KDM5A/B is much higher in Dox-treated *vs* un-treated TREx.BCBL-1.RTA cells in the
103 presence of MG132 (**Fig 1H, 1I**), while their K63-linked polyubiquitination was not detected.
104 Early studies indicated that KSHV RTA promotes the protein degradation of certain host factors
105 through upregulation of their K48-linked polyubiquitination(19,20). We employed the KSHV-
106 negative BJAB cells carrying a cassette for Dox induced expression of 3 × FLAG-tagged RTA
107 (TREx.BJAB.3FLAG.RTA) to determine whether RTA directly mediates KDM5 protein
108 degradation. However, Dox treatment failed to decrease KDM5 proteins in these cells (**Fig S1J**).
109 Transfection of RTA cDNA in HEK293T cells also failed to do so with or without MG132 (**Fig**
110 **S1K**). Overall, our results demonstrated that KSHV lytic replication promotes proteosome
111 degradation of KDM5 proteins (KDM5A-C), which may depend on other KSHV viral lytic
112 components/events beyond RTA.
113 **KDM5A/B suppress KSHV lytic reactivation from latency.** In light of our early findings
114 of KDM5A/B's role in silencing HIV proviruses, we were curious whether KDM5A/B impact
115 the lytic/latent switch of KSHV as well. TREx.BCBL-1.RTA cells were electroporated with

116 siRNAs targeting KDM5A, KDM5B, or KDM5C, followed by Dox treatment. KDM5A/B were
117 efficiently depleted (**Fig 2A, 2B**), which significantly promoted the Dox-induced KSHV lytic
118 reactivation (**Fig 2C-F**). However, knockdown of KDM5C showed no such effects (**Fig S2A**,
119 **S2B**). We also confirmed these findings in the iSLK.BAC16 cells, a human renal cell carcinoma
120 cell line with the epithelial cell origin (SLK) that harbors a bacterial artificial chromosome clone
121 (BAC16) of the recombinant KSHV genome while also carrying an integrated cassette for Dox
122 induced RTA expression. Similarly, KDM5A/B depletion by siRNAs dramatically promoted the
123 Dox-induced KSHV lytic reactivation in iSLK.BAC16 cells (**Fig 2G-L**). Such phenotypes were
124 also observed in another iSLK cell model of KSHV, the iSLK.r219 cells harboring the KSHV
125 r219 strain that expresses RFP from KSHV lytic PAN promoter as well as GFP constitutively
126 from the EF1a promoter. KDM5A/B depletion by either siRNAs or shRNAs remarkably
127 increased the RFP florescence intensity in iSLK.r219 cells (**Fig 2M, 2N, S2C, S2D**). Thus, we
128 demonstrated that KDM5A/B but not KDM5C play a role in blocking KSHV lytic reactivation
129 from latency.

130 **KDM5A/B associate with KSHV LANA and modulate its functions.** LANA is a KSHV-
131 encoded oncoprotein critical to maintain viral latency as well as drive viral tumorigenesis(21). A
132 report showed that chromatin association of KSHV LANA overlaps significantly with that of
133 H3K4me3(22), the major substrate of KDM5A/B. We re-analyzed the public-domain chromatin
134 immunoprecipitation followed by sequencing (ChIP-seq) data generated in BC3 cells
135 (GSE202670). We compared the ChIP-seq peaks of H3K4me3 with host (DNA Polymerase I
136 alpha) and KSHV viral proteins (LANA, RTA) extracted from the raw datasets. Average profile
137 plot of ChIP-seq peaks showed the similar patterns only between LANA and H3K4me3 (**Fig 3A**)
138 as opposed to RTA and DNA Polymerase I alpha. We further focused on their binding peaks

139 particularly at loci of immune-responsive genes (IRGs). Profile plots and heatmaps of IRG peaks
140 showed the highly concordant patterns only between LANA and H3K4me3 (**Fig 3B**). The peak
141 overlap enrichment analysis between LANA and H3K4me3 at IRGs was significant with
142 adjusted *P*-value ($P = 0.0192$). These data analyses indicated a cooperative association between
143 LANA and KDM5A/B-targeted H3K4me3 mark to regulate viral and host gene expression,
144 including IRGs. To prove this, we first confirmed that KSHV LANA protein interacts with
145 endogenous KDM5A/B proteins in BCBL-1 cells by protein immunoprecipitations (**Fig 3C**).
146 Such protein interactions were also verified in iSLK.BAC16 cells by both protein
147 immunoprecipitations (**Fig 3D**) and protein colocalization (**Fig 3E, 3F**). KDM5A/B remained to
148 bind with LANA despite that their protein level significantly decreased upon KSHV lytic
149 reactivation in Dox-treated TREx.BCBL-1.RTA (**Fig S3A**) and iSLK.BAC16 (**Fig S3B, S3C**)
150 cells.

151 We next determined whether KDM5A/B interact with LANA to modulate its functions.
152 Depletion of KDM5A/B by their siRNAs only modestly decreased the protein expression of a
153 LANA cDNA transfected in the HEK293T (**Fig S3D**). LANA has been reported to promote
154 KSHV latency through binding to viral lytic promoter that controls RTA expression and
155 suppressing its activities(23-25). We showed that the chromatin association of LANA at RTA
156 promotor significantly decreased in iSLK.BAC16 cells due to KDM5A/B depletion by siRNAs
157 (**Fig 3G**). Furthermore, LANA has also been reported to directly suppress the expression of
158 certain host antiviral genes to favor KSHV viral persistent infection(26,27). It has been
159 implicated that LANA directly associates at the promoter of immune genes to regulate their
160 expression(28), which aligned with our data analysis of LANA ChIP-seq data as well (**Fig 3B**).
161 We demonstrated that KDM5A/B depletion by siRNAs indeed caused a remarkable reduction of

162 LANA's chromatin association at the promotor of several antiviral immune genes ((**Fig 3H**).
163 Overall, we identified that KDM5A/B associate with KSHV LANA, which showed no obvious
164 impact on LANA protein expression but determined LANA's chromatin association and its
165 functions to promote KSHV viral latency.

166 **KDM5 inhibition induces KSHV lytic reactivation from latency.** As our own data showed
167 that KDM5A/B prevent latent KSHV from lytic reactivation likely through interaction with
168 LANA to modulate its functions, we speculated that their inhibition would promote KSHV lytic
169 reactivation in KSHV-infected tumor cells and induce the viral oncolysis effect. Recently, a
170 KDM5-specific inhibitor JQKD82 has been developed, which is a prodrug of KDM5-C49(29)
171 and has demonstrated the antitumor potency against multiple myeloma(30). JQKD82 treatment
172 significantly enhanced Dox-induced KSHV lytic reactivation in TREx.BCBL-1.RTA cells by
173 quantifying viral lytic gene expression at the doses with no obvious cytotoxicity (**Fig 4A-C**).
174 Such findings were confirmed by using another KDM5-specific inhibitor CPI-455 that exerted
175 the similar effects on Dox-induced KSHV lytic reactivation in TREx.BCBL-1.RTA cells (**Fig**
176 **S4A, S4B**). We further tested JQKD82 using KSHV-positive PEL cell lines that harbor latent
177 KSHV, including BCBL-1 and BC-3. JQKD82 alone was competent to potently induce KSHV
178 lytic reactivation in these cells at different doses (**Fig 4D, 4E, S4C, S4D**). Regardless of cell
179 types, JQKD82 still remarkedly promoted Dox-induced KSHV lytic reactivation in iSLK.BAC16
180 cells (**Fig 4F, 4G**). On the contrary, JQKD82 treatment only slightly decreased the protein
181 expression of a LANA cDNA transfected in HEK293T cells while increasing the total level of
182 H3K4me3 (**Fig S4E**). Therefore, our results illustrated the potential to use KDM5 inhibitors for
183 reversal of latent KSHV that would further lead to viral oncolysis for KSHV-positive B-cell
184 lymphomas.

185 **KDM5 inhibition induces antiviral/antitumor innate immune responses.** During KSHV
186 lytic reactivation from latency, host innate immune responses are also activated, which is
187 expected to favor the tumor cell killing by generating the additional oncolytic effects(9). We thus
188 performed the transcriptome profiling analysis for both KSHV-infected BCBL-1 *vs* KSHV-
189 negative BJAB cells with or without JQKD82 treatment by RNA-seq. Although JQKD82
190 induced the expression of several well-defined antiviral/antitumor IRGs, including IRF6, IRF7,
191 and OAS1, in both BCBL-1 and BJAB cells (**Fig 5A, 5B**), such immune activation was much
192 stronger in BCBL-1 cells indicated by the pathway analysis showing that several immune-related
193 pathways are enriched in JQKD82-treated BCBL-1 cells (**Fig 5C**) but not BJAB (**Fig S5A**).
194 We then focused on a set of highly upregulated IRGs in JQKD82-treated BCBL-1 cells for
195 experimental validation by RT-qPCR assays (**Fig 5D**). We first quantified the mRNAs of IRGs
196 identified in both JQKD82-treated BCBL-1 and BJAB cells (IRF6, IRF7, OAS1), which have
197 been reported to suppress tumor growth(31-33). JQKD82 preferentially caused the induction of
198 these IRGs in BCBL-1 (**Fig 5E**) compared to BJAB (**Fig S5B**) cells. We further validated
199 additional antiviral/antitumor IRGs, including IFNγ, IRF8, and MX2, which were enriched only
200 in JQKD82-treated BCBL-1 cells identified from RNA-seq analysis. Along with induction of
201 KSHV lytic gene K8 (**Fig 5F**), these additional IRGs were also preferentially induced in
202 JQKD82-treated BCBL-1 (**Fig 5G**) in comparison to BJAB (**Fig S5C**) cells. Therefore, our
203 transcriptome profiling analysis and further experimental validation suggested that the KDM5
204 inhibitor JQKD82 is capable of inducing antiviral/antitumor innate immune responses in KSHV-
205 negative B-cell lymphomas, but such effects are more striking in KSHV-positive B-cell
206 lymphomas likely due to KSHV lytic reactivation that further triggers the innate immune
207 activation in tumor cells.

208 **KDM5 inhibition promotes the death of KSHV-positive PEL cells *in vitro*.** Since
209 JQKD82 was capable of inducing viral oncolytic effects and antiviral/antitumor immune
210 responses in KSHV-positive B-cell lymphomas, we next evaluated the drug's potential to treat
211 these tumors. To establish the clinical relevance of KDM5 proteins as targets for anticancer
212 treatment, we first compared their protein expressions between malignant and normal B cells. In
213 contrast to BJAB cells, KDM5 proteins (KDM5A-C) barely expressed in the $CD19^{+}CD3^{-}$
214 primary B cells isolated from three healthy donors (**Fig 6A, S6A, S6B, S6C**). However, KDM5
215 protein expressions varied across KSHV-negative BL (BJAB, Ramos) and KSHV-positive PEL
216 (BCBL-1, BC-3) cell lines (**Fig 6B, S6D**). We also performed the protein immunofluorescence
217 assays (IFA) of KDM5A/B using the lymph node tissues from the deidentified, two donors of
218 diffuse large B-cell lymphoma (DLBCL) and two healthy donors, which showed that KDM5A/B
219 proteins highly express in tumorous *vs* normal lymph nodes (**Fig 6C, 6D**). These findings
220 implicated that KDM5 proteins may serve as promising antitumor targets for treating various
221 subtypes of Non-Hodgkin B-cell lymphomas (NHL), including KSHV-associated ones.
222 We then determined JQKD82's anticancer effects on inducing the cytotoxicity/death of
223 KSHV-positive PEL cells (BCBL-1, BC-3) as well as KSHV-negative BJAB cells using normal
224 B cells as a reference. These cells were cultured up to 5 days with JQKD82 treatment at different
225 doses (5-50 μM). First, our results showed that JQKD82 causes no or only mild cytotoxicity of
226 BJAB cells while even increasing the viability of normal B cells despite of the high doses of
227 JQKD82 (**Fig 6E, S6E**). Second, in contrast to BJAB cells JQKD82 treatment indeed rendered
228 the more obvious cytotoxicity/death of BCBL-1 (**Fig 6F**) and BC-3 (**Fig 6G**) cells across all-
229 tested drug concentrations *in vitro*. Thus, these studies recognized that KDM5 inhibition could
230 be considered as a viable strategy to preferentially treat KSHV-positive B-cell lymphomas.

231 **KDM5 inhibition blocks the tumor growth of KSHV-positive PEL cells *in vivo*.** Given
232 JQKD82 elicited potent antitumor effects on KSHV-positive PEL *in vitro*, we further evaluated
233 this compound on tumor growth *in vivo* using a PEL xenograft mouse model (**Fig 7A**). The NSG
234 mice were transplanted intraperitoneally (i.p.) with the BCBL-1 cells that stably express an
235 integrated cassette of firefly luciferase (BCBL-1-Luc), which allowed the bioluminescence
236 imaging (BLI) to monitor the tumor growth in live animals over the time. The results showed
237 that JQKD82 dramatically inhibits the growth of KSHV-positive PEL in mice during BLI
238 monitoring twice a week up to 28 days post of tumor transplantation in comparison to vehicle
239 control (**Fig 7B, 7C**). The mice were sacrificed, and the tumors and ascites were collected for
240 measurements. JQKD82 treatment substantially decreased the tumor size/volume (**Fig 7D, 7E**),
241 tumor weight (**Fig 7F**), and ascites volume (**Fig 7G**). However, JQKD82 only moderately
242 affected the body weight of PEL-transplanted mice comparing to vehicle control (**Fig S7A**). For
243 the collected tumor samples, we further quantified JQKD82's drug effects on viral and immune
244 gene expressions by RT-qPCR assays. Consistent with the *in vitro* findings, JQKD82
245 administration indeed induced KSHV viral gene expressions in tumors (**Fig 7H, S7B**). Likewise,
246 JQKD82 upregulated the expression of anti-tumor IRGs in tumors as well (**Fig 7I, S7C**). Overall,
247 our *in vivo* evaluations clearly demonstrated the therapeutic promise of KDM5 inhibitor JQKD82
248 to treat KSHV-associated B-cell lymphomas through induction of viral oncolysis.
249

250 **Discussion**

251 The viral life cycle of KSHV includes latent and lytic replications as two distinct phases that
252 are delicately controlled by both viral and host factors, assuring KSHV to not only establish
253 persistent infection and escape immune surveillance in the host cells but also generate new

254 progeny viruses once reactivated for viral dissemination and transmission to the new hosts(34).
255 KSHV also encodes an array of viral oncogenes that promote host cell's transformation and
256 contribute to the development of KSHV-associated malignancies(35). Therefore, elucidation of
257 profound KSHV-host interactions is necessary to advance the understanding of KSHV viral life
258 cycle as well as KSHV-induced tumorigenesis, which would lead to the identification of new
259 gene targets for developing potent and specific anti-KSHV agents. In this study, we provided the
260 novel findings that KDM5A/B proteins play a previously unappreciated role in suppressing
261 KSHV lytic reactivation from latency (**Fig 2**) while KSHV may temporarily downregulate these
262 demethylases via proteosome degradation during its lytic replication to benefit viral propagation
263 (**Fig 1**).

264 KDM5 family includes four members KDM5A-D, which are the Jumonji-C (JmjC) domain-
265 containing lysine demethylases and catalyze the removal of methyl groups from the epigenetic
266 marks of gene activation H3K4me2/3(36). There is growing evidence showing that KDM5A/B
267 play critical roles in cancer development(15). For example, KDM5A/B are overexpressed in
268 breast cancer(37,38). Loss of KDM5A sensitized the endocrine-resistant luminal breast cancer
269 cells to fulvestrant(39), while loss of KDM5B reduced the proliferation of breast cancer cells *in*
270 *vivo*(40). Upregulation of KDM5A/B has been observed in multiple types of cancers, such as
271 gastric cancer(41,42), head and neck cancer(43,44), lung cancer(45,46), indicating their strong
272 connections to cancer development. So far, only few reports have linked KDM5A/B proteins to
273 B-cell lymphomas, such as mantle cell lymphoma (MCL) and germinal center (GC)
274 lymphoma(47,48). In contrast, KDM5C/D locate on X and Y chromosomes, respectively, which
275 have been linked to sex-dependent conditions, such as X-linked intellectual disability (XLID),
276 autism, and certain types of sex-specific cancers(49-51). The main B-cell lines we used for this

277 study were mostly generated from BCBL-1 that was derived from an adult male but with an
278 acquired, complete loss of the Y chromosome, while the KSHV-negative BJAB was established
279 from a 5-year-old African girl. Thus, we excluded KDM5D from out studies. Interestingly, we
280 found that although KSHV lytic replication decreases KDM5C protein (**Fig S1B, S1H**), its
281 depletion fails to induce KSHV lytic reactivation (**Fig S2A, S2B**). Since KDM5C may share
282 certain conserved protein domains with KDM5A/B required for KSHV-mediated proteosome
283 degradation, KDM5C is thus also subjected to such dysregulation. However, more likely
284 KDM5A/B play the dominant roles in controlling KSHV viral life cycle.

285 Our mechanistic investigations identified that KDMA5A/B interaction with LANA may
286 contribute to its functions that promote KSHV viral latency and immune escape to benefit its
287 persistent infection (**Fig 3, S3**). As a pivotal viral factor, KSHV LANA is known to modulate
288 both viral and host gene expression by interacting with cellular proteins, including epigenetic
289 regulators. Early studies have demonstrated that LANA associates with the KSHV viral lytic
290 promoter and negatively regulate its functions to drive the activation of KSHV viral trans-
291 activator RTA that further induces a cascade of KSHV lytic gene expression(23). Indeed,
292 depletion of KDM5A/B significantly decreased LANA chromatin association at the RTA
293 promoter (**Fig 3G**). Furthermore, LANA has also been reported to suppress antiviral/antitumor
294 innate immune responses(26,27). Our data mining provided the supportive evidence that
295 chromatin occupancy of LANA significantly overlaps with that of H3K4me3 at IRG loci (**Fig**
296 **3B**). We showed that depletion of KDM5A/B substantially reduces LANA chromatin association
297 at the promoter of IRGs (**Fig 3H**). It is thus plausible that KSHV targets KDM5A/B for
298 proteosome degradation, which would alleviate LANA suppression of RTA activation during
299 viral lytic reactivation. On the other hand, KSHV-mediated KDM5A/B downregulation would

300 also alleviate LANA suppression of antiviral/antitumor IRG activation, resulting in a viral
301 oncolytic impact. Although we ruled out that RTA possesses the functions to induce proteosome
302 degradation of KDM5A/B (**Fig S1J, S1K**), It remains to be identified which viral and/or cellular
303 mechanisms employed by KSHV to do so.

304 The fundamental understanding of KDM5A/B's functions to control KSHV viral replications
305 and anti-KSHV innate immune responses would lay the foundation to target them by using
306 small-molecule inhibitors for treating KSHV-associated cancers. KDM5 inhibitors, such as
307 KDM5-C49 or KDM5-C70, have been shown to sensitize endocrine-resistant luminal breast
308 cancer cells to fulvestrant, and the combination of fulvestrant and KDM5 inhibitor substantially
309 reduced tumor volume(39). Although the incidence is rare, KSHV highly associates with certain
310 types of B-cell lymphomas(52), such as PEL, which have the overall lower survival rate than
311 other common types of aggressive B-cell lymphomas(53), leading to short median survival time
312 (only 6-22 months) and poor 5-year survival rate (less than 17%). Although certain treatments
313 extrapolated from other common types of B-cell lymphomas have been applied to PEL and
314 improved its survival rate, there are still no specific therapies developed against these KSHV-
315 associated B-cell lymphomas. Based on our own studies, KDM5A/B would be the ideal targets
316 for treating B-cell lymphomas, as they appeared to preferentially express in malignant *vs* normal
317 B cells (**Fig 6A-D, S6C, S6D**). As a proof of concept, we demonstrated that a recently available
318 KDM5 inhibitor JQKD82 is potent to induce KSHV lytic reactivation and activate
319 antiviral/antitumor innate immune responses in KSHV-infected PEL cells both *in vitro* (**Fig 6**)
320 and *in vivo* (**Fig 7**), facilitating their killing. Such viral oncolytic approaches could be considered
321 for treating other virus-associated cancers. For example, we showed that JQKD82 is capable of
322 inducing lytic reactivation of another human gamma-herpesvirus Epstein-Barr Virus (EBV) and

323 preferentially kills EBV-positive BL cells (BL41-P3HR1) *vs* the parental BL41 (**Fig S7D-F**).
324 However, a limitation is that our NSG mouse model lacks proper immune systems. In future, we
325 will consider using the humanized mouse model with PEL xenograft for further evaluation of
326 KDM5 inhibitor's impact on antitumor immunity.
327

328 **Materials and Methods**

329 **Cells.** Cell lines of B-cell lymphomas, including BJAB, Ramos, BL41, BL41-P3HR1,
330 TREx.BJAB.3FLAG.RTA, BCBL-1, BCBL-1-Luc, TREx.BCBL-1.RTA, were maintained in
331 RPMI 1640 medium (Gibco) supplemented with 10% fetal bovine serum (FBS) (Gibco). BC-3
332 cells were maintained in RPMI 1640 medium supplemented with 20% FBS. iSLK.BAC16,
333 iSLK.r219, HEK293T cells were maintained in Dulbecco's modified Eagle's medium (DMEM)
334 (Gibco) supplemented with 10% FBS. Antibiotics were added in cell cultures for TREx.BCBL-
335 1.RTA and TREx.BJAB.3FLAG.RTA (200 μg/mL Hygromycin B), BCBL-1-Luc (50 μg/mL
336 Hygromycin B), iSLK.BAC16 and iSLK.r219 (1.2 mg/mL Hygromycin B, 2 μg/mL puromycin,
337 250 μg/mL G418) as previously described(54). Telomerase-immortalized human microvascular
338 endothelial (TIME) cells were maintained in Vascular Cell Basal Medium (ATCC, Cat# PCS-
339 100-030) supplemented with Microvascular Endothelial Cell Growth Kit-VEGF (ATCC, Cat#
340 PCS-100-041). Human primary cells, including peripheral blood mononuclear cells (PBMCs)
341 (STEMCELL Technologies) as well as the isolated B cells, were maintained in RPMI 1640
342 complete medium (RPMI 1640 basic, 1× MEM Non-Essential Amino Acids Solution, 1×
343 Sodium Pyruvate, and 20 mM HEPES) supplemented with human recombinant IL-2 (rIL-2,
344 Roche) at 30 U/mL. Human $CD19^{+}CD3^{-}$ primary B cells were isolated from PBMCs using the B

345 cell Isolation Kit II (Miltenyi Biotec, Cat# 130-091-151) according to the manufacturer's
346 protocol.

347 **Reagents and antibodies.** Doxycycline was purchased from Fisher Scientific (Cat# BP2653-
348 1). DMSO for *in vitro* assays was purchased from Fisher Scientific (Cat# BP231-100). DMSO
349 for *in vivo* applications was purchased from MP Biomedicals (Cat# 2780148). KDM5 inhibitor
350 JQKD82 for *in vitro* experiments was designed, synthesized, and kindly provided by Dr. Jun
351 Qi's lab at Dana-Farber Cancer Institute(30). JQKD82 for *in vivo* administrations was purchased
352 from Cayman (Cat# 41542). siRNAs targeting KDM5A-C or non-targeting (NT) siRNA were
353 purchased from Invitrogen. Human IgG was purchased from MP Biomedicals (Cat# 55087).
354 MG132 was purchased from Sigma-Aldrich (Cat# 474790). The following antibodies were used
355 in this study: anti-KDM5A (Active Motif, Cat# 91211); anti-KDM5B (Bethyl Laboratories, Cat#
356 A301-813A); ant-KDM5C (Bethyl Laboratories, Cat# A301-034A); anti-KSHV K8.1 (Santa
357 Cruz Biotechnology, Cat# sc-65446); anti-EBV EBNA1 (Santa Cruz Biotechnology, Cat# sc-
358 81581); anti-GAPDH (Santa Cruz Biotechnology, Cat# sc-47724); normal rat IgG (Santa Cruz
359 Biotechnology, Cat# sc-2026); anti-KSHV LANA (Advanced Biotechnologies, Cat# 13-210-
360 100); anti-FLAG M2 (Sigma-Aldrich, Cat# F1804); anti-CD3-FITC (Miltenyi Biotec, Cat# 130-
361 113-690); anti-CD19-PE (Santa Cruz Biotechnology, Cat# 130-113-731); anti-CD20 (BioLegend,
362 Cat# 382802); anti-mouse HRP-linked (Cell Signaling Technology, Cat#7076S) and anti-rabbit
363 HRP-linked (Santa Cruz Biotechnology, Cat# 7074S) antibodies; isotype control IgG including
364 rabbit IgG (Santa Cruz Biotechnology, Cat# 3900S), mouse IgG_1 (Santa Cruz Biotechnology,
365 Cat# 5415S), mouse IgG_{2a} (Santa Cruz Biotechnology, Cat# 61656S) and mouse IgG_{2b} (Santa
366 Cruz Biotechnology, Cat# 53484S).

367 **Protein immunoblotting and immunoprecipitation assays.** Protein immunoblotting and
368 immunoprecipitation (IP) assays were performed as previously described(55). Briefly, total
369 proteins were extracted from cell lysates by using 1 × radioimmunoprecipitation assay (RIPA)
370 buffer (MilliporeSigma, Cat# 20-188) containing broad-spectrum protease inhibitors (Thermo
371 Scientific, Cat# A32953). Protein concentrations were measured using a BCA assay kit (Thermo
372 Scientific, Cat# 23227), followed by electrophoresis and dry electro-transfer. The PVDF
373 membrane was blocked with nonfat milk, and incubated with primary and HRP-conjugated
374 secondary antibodies, followed by the incubation with ECL substrate for chemiluminescence. To
375 determine protein-protein interactions, cell lysates were incubated with the specific antibodies
376 recognizing the targeted proteins or control IgG, followed by the incubation with protein A/G
377 magnetic beads (Thermo Scientific, Cat# 88803). Beads containing protein immunocomplexes
378 were washed, eluted, and subjected to protein immunoblotting assay. Gel images were acquired
379 by the ProteinSimple FluorChem E Imaging System.

380 **Protein immunofluorescence assay (IFA).** Primary B cell isolations were evaluated by IFA,
381 followed by flow cytometry analysis as previously described(56). Original PBMCs as well as
382 isolated B cells were incubated with anti-CD3-FITC and anti-CD19-PE antibodies for 30 mins,
383 which were subjected to flow cytometry analysis using BD Accuri C6 Plus. B cell population
384 ($CD19^+/CD3^-$) was analyzed by the FlowJo V10 software. KSHV LANA and KDM5A/B protein
385 interactions were also determined by IFA. iSLK.BAC16 cells were seeded at 1.5×10^5 cells per
386 well on a 24-well culture plate containing circular cover glasses (13 mm) 1 day prior to the
387 induction of KSHV lytic reactivation. Cells were treated with Dox (1 μg/mL) for 2 days. Cells
388 were then fixed with 4% paraformaldehyde at room temperature (RT) for 10 min, followed by
389 permeabilization with 0.2% Triton X-100 at RT for 15 min. The fixed cells were blocked with 1×

390 D-PBS containing 5% FBS for 1 hour at RT and incubated with the primary antibodies (LANA
391 and KDM5A/B) in 1× D-PBS containing 2.5% FBS overnight at 4°C. Anti-rat Alexa Fluor 488
392 or anti-mouse/rabbit Alexa Fluor 647 conjugated secondary antibodies were then added to cells
393 for another incubation for 1 hour at RT with constant rocking. Nuclei were stained with Hoechst
394 33342 (Thermo Scientific, Cat# 62249) for 10 min at RT. The cover glasses containing cells
395 were mounted onto a microscope slide with ProLong Glass Antifade Mountant (Invitrogen, Cat#
396 P36980), followed by incubation overnight at 4°C in the dark. Images were acquired using a
397 ZEISS LSM 700 Upright laser scanning confocal microscope with a ZEN imaging software
398 (ZEISS). To quantify KSHV lytic reactivation or *de novo* infection rate, cell samples in culture
399 plates were washed with 1x D-PBS followed by fluorescence imaging using the Cytation 5
400 multi-mode reader and the Gen5 Image+ software (BioTek).

401 **Chromatin immunoprecipitation (ChIP).** ChIP assays were performed as previously
402 described(57). In brief, 1% paraformaldehyde (PFA) was used for cell cross-linking. Cells were
403 then re-suspended by CE buffer and centrifuged to pellet nuclei, which were further incubated
404 with SDS lysis buffer and sonicated to shear DNA fragments. 4% of nuclear lysates were used as
405 the Input, and the remaining lysates were incubated with antibodies recognizing the targeted
406 proteins or control IgG, followed by the incubation with pre-blocked protein A/G magnetic beads.
407 The beads were sequentially washed with low-salt buffer, high-salt buffer, LiCl buffer, and TE
408 buffer, and the IPed protein-DNA complexes were isolated by elution buffer. To recover DNA
409 samples, the elutes were treated with 5 M NaCl and incubated at 65 °C for overnight, followed
410 by the treatment of EDTA, Tris-HCl (pH 6.5), and proteinase K. DNA samples were extracted
411 by phenol/chloroform/isoamyl alcohol (25:24:1). DNA pellets were re-suspended in nuclease-

412 free water, which were used for qPCR analysis. The primers used for ChIP-qPCR assays were
413 listed in the supplementary table **(Table S1)**.

414 **Cell viability assay.** ATP-based CellTiter-Glo Luminescent Cell Viability Assay (Promega)
415 was used to measure drug-induced cytotoxicity following the manufacturer's instructions.
416 Luminescence was measured by the Cytation 5 multimode reader (BioTek).

417 **KSHV viral propagation and infection.** KSHV BAC16 viruses were propagated as
418 previously described with slight modifications(54,56). In brief, iSLK.BAC16 cells were treated
419 with 2 μg/mL doxycycline together with 1 mM sodium butyrate (NaB) for 24 h to reactivate
420 KSHV. Cells were then maintained in fresh medium containing 2 μg/mL doxycycline, and the
421 supernatants containing KSHV BAC16 viruses were harvested every 2 days. Total five batches
422 of harvested supernatants were collected, centrifuged (400 × g) for 10 mins to remove cell debris,
423 and filtered through the 0.45 μm filter. KSHV BAC16 viruses were titrated in HEK293T cells
424 through the serial dilutions. Pre-seeded cells were infected with KSHV BAC16 viruses via
425 spinoculation (2500 rpm) for 2 h at 37 °C.

426 **Protein immunohistochemistry (IHC) assay**. The lymph node specimens from deidentified
427 healthy donors or DLBCL patients were fixed with 4% paraformaldehyde (PFA) at 4°C for
428 overnight, dehydrated through a series of grade ethanol, and incubated with Histo-Clear
429 (National Diagnostics, Cat# 5989-27-5) at room temperature for 2 h prior to paraffin embedding.
430 7 μm thick sections were then prepared from the paraffin blocks and mounted on the slides. Such
431 paraffin-embedded tissue slides were baked in a high temperature incubator at 65 °C for 30 min
432 and deparaffinized in xylene. The slides were sequentially rehydrated in 100%, 95%, 70%, 50%
433 ethanol and PBS, followed by the antigen unmasking using a pressure cooker with 1 × antigen
434 retrieval buffer (Abcam, Cat# AB93684) for 2 h to complete the cycle and then cool down.

435 Slides were permeabilized with 0.5% Triton X-100 in PBS for 10 min and blocked with 10%
436 normal goat serum (NGS) in 1x PBST for 2 h at room temperature, then incubated with anti-
437 KDM5A, anti-KDM5B, and anti-CD20 antibodies in 5% NGS with 1x PBST at 4°C for
438 overnight. Fluorophore-conjugated secondary antibodies (Alexa Fluor 488 or Alexa Fluor 647)
439 were diluted in 5% NGS with 1x PBST and incubated with the tissue slides for 2 h at room
440 temperature in the dark. These slides were then stained with Hoechst (1:6000 in PBST, Thermo
441 Scientific, Cat# 62249) for 10 min at room temperature, followed by mounting with coverslips
442 using ProLong Glass Antifade Mountant (Invitrogen, Cat# P36982) and curing for overnight.
443 Images were acquired using the ZEISS LSM 700 Upright laser scanning confocal microscope
444 and ZEN imaging software (ZEISS).

445 **Quantitative reverse transcription PCR (RT-qPCR).** Total RNAs were extracted from
446 cells by using the NucleoSpin RNA isolation kit (MACHEREY-NAGEL, Cat# 740955.250).
447 Eluted RNA samples were reverse transcribed by using the iScript cDNA Synthesis Kit (Bio-Rad,
448 Cat# 1708891) following the manufacturer's instructions. RT-qPCR assays were performed by
449 using the iTaq Universal SYBR Green Supermix (Bio-Rad, Cat# 1725125) on a Bio-Rad CFX
450 Connect Real-Time PCR System. The primers used for RT-qPCR assays were listed in **Table S1**.

451 **RNA-seq analysis.** BCBL-1 and BJAB cells were treated with JQKD82 (20 μM) or DMSO
452 for 4 days. RNA samples from three independent repeats were extracted by using the NucleoSpin
453 RNA isolation kit following the manufacturer's manual. RNA samples were submitted to
454 Novogene (Sacramento, CA 95817) for further library preparations. RNA samples that passed
455 quality control were subjected to rRNA removal through polyA selection, followed by the
456 generation of cDNA libraries. Sequencing was carried out on an Illumina NovaSeq X Plus
457 platform with the configuration of 2 × 150 bp (paired end). Differential expression of genes was

458 analyzed by DESeq2(58). R packages, EnhancedVolcano, pheatmap and clusterProfiler
459 programs were used for volcano plotting, heatmap construction and pathway analysis,
460 respectively. The differentially expressed genes (DEGs) in BCBL-1 and BJAB cells due to
461 JQKD82 treatment were listed in the supplementary tables **(Table S2, S3),** respectively. These
462 RNA-seq datasets were deposited in the Gene Expression Omnibus (GEO) with the accession
463 number GSE310839.

464 **A PEL xenograft mouse model.** A PEL xenograft mouse model was employed to determine
465 the antitumor effect of a KDM5 inhibitor JQKD82 on the growth of KHSV-infected PEL cells *in*
466 *vivo*. Six-week-old female NOD.Cg-*Prkdc*^{scid} *Il2rg*^{tm1Wjl}/SzJ (NSG) mice were acquired from the
467 Ohio State University Comprehensive Cancer Center and transplanted with 5×10^6 of BCBL-1-
468 Luc cells intraperitoneally (i.p.) per mouse. One week post of tumor xenograft, mice were
469 injected i.p. with D-Luciferin (GoldBio, cat# LUCK-1G) and subjected to the bioluminescence
470 imaging (BLI) for monitoring tumor growth using the IVIS Spectrum 2 In Vivo Imaging System
471 (Revvity). These mice were randomized and grouped for administration with either vehicle
472 control or JQKD82 (50 mg/kg) every two days for two weeks (4 mice per group). The JQKD82
473 solution was prepared as previously described(30). Briefly, JQKD82 was dissolved in DMSO to
474 prepare the 50 mg/mL solution, which was then further diluted in the 2-Hydroxypropyl)-β-
475 cyclodextrin (Sigma-Aldrich, cat# 332607) with 1:9 ratio (5 mg/mL) for *in vivo* administration.
476 Tumor burden in these mice was monitored by BLI up to three weeks. All mice were euthanized,
477 and tumor samples were collected for further measurements. These animal studies were
478 approved by the Ohio State University Institutional Animal Care and Use Committee (IACUC).

479 **Statistical analysis**. The experimental data were acquired from at least three independent
480 repeats, and analyzed by using either the unpaired, two-tailed/one-tailed Student's t test or the

481 one-way/two-way analysis of variance (ANOVA). A *P*-value less than 0.05 was considered as
482 statistically significant (*$P < 0.05$, **$P < 0.01$, ***$P < 0.001$, ****$P < 0.0001$). Results were
483 presented as either Mean ± standard deviation (SD) or Mean ± standard error of the mean (SEM),
484 and graphed by using the GraphPad Prism 9.0 software.
485

486 **Acknowledgments**

487 We would like to thank Dr. Renfeng Li (University of Pittsburgh) for providing BJAB cells,
488 Dr. Jae Jung (Cleveland Clinic) for TREx.BCBL-1.RTA cells, Dr. Zsolt Toth (University of
489 Florida) for TREx.BJAB.3FLAG.RTA cells, Dr. Shou-Jiang Gao (University of Pittsburgh) for
490 iSLK.BAC16, iSLK.r219, and TIME cells, Dr. Erle Robertson (University of Pennsylvania) for
491 pA3M-LANA plasmid, and Dr. Robert Baiocchi (Ohio State University) for BL41 and BL41-
492 P3HR1 cells. This study was supported by NIH research grants R01CA260690 to
493 N.S.; R01MH134402, R01DA059538, and R56AI181631 to J.Z.
494

495 **Author contributions**

496 N.G.S., J.Z. and D.Z. conceived and designed this study; D.Z. performed the majority of
497 experiments; G.N.F. and S.E. provided experimental supports; Z.W. performed the RNA-seq
498 data analysis; D.Z., N.G.S. and J.Z. analyzed the results; Y.P., J.H., K.A.S.N.S., T.T.L., Y.L.,
499 J.O., K.L., J.U.J., J.Q., W.J.Z. contributed materials and/or provided advice for this study; D.Z.,
500 N.G.S., J.Z. wrote the manuscript; N.G.S. and J.Z. supervised the entire study.
501

502 **Competing interests**

503 The authors declare no competing interests.

504

505 **Data and materials availability**

506 All data are presented in the main manuscript and/or as the supplementary materials. All
507 other related data, information, and materials can be acquired through the direct requests to
508 authors.

509 **References**

510 1. Antman, K. and Chang, Y. (2000) Kaposi's sarcoma. *N Engl J Med*, **342**, 1027-1038.
511 2. Cesarman, E., Chang, Y., Moore, P.S., Said, J.W. and Knowles, D.M. (1995) Kaposi's
512 sarcoma-associated herpesvirus-like DNA sequences in AIDS-related body-cavity-based
513 lymphomas. *N Engl J Med*, **332**, 1186-1191.
514 3. Soulier, J., Grollet, L., Oksenhendler, E., Cacoub, P., Cazals-Hatem, D., Babinet, P.,
515 d'Agay, M.F., Clauvel, J.P., Raphael, M., Degos, L. *et al.* (1995) Kaposi's sarcoma-
516 associated herpesvirus-like DNA sequences in multicentric Castleman's disease. *Blood*,
517 **86**, 1276-1280.
518 4. Means, R.E., Lang, S.M. and Jung, J.U. (2007) In Arvin, A., Campadelli-Fiume, G.,
519 Mocarski, E., Moore, P. S., Roizman, B., Whitley, R. and Yamanishi, K. (eds.), *Human*
520 *Herpesviruses: Biology, Therapy, and Immunoprophylaxis*, Cambridge.
521 5. Longnecker, R. and Neipel, F. (2007) In Arvin, A., Campadelli-Fiume, G., Mocarski, E.,
522 Moore, P. S., Roizman, B., Whitley, R. and Yamanishi, K. (eds.), *Human Herpesviruses:*
523 *Biology, Therapy, and Immunoprophylaxis*, Cambridge.
524 6. Sandhu, P.K. and Damania, B. (2022) The regulation of KSHV lytic reactivation by viral
525 and cellular factors. *Curr Opin Virol*, **52**, 39-47.
526 7. Cohen, J.I. (2020) Herpesvirus latency. *J Clin Invest*, **130**, 3361-3369.
527 8. Lieberman, P.M. (2013) Keeping it quiet: chromatin control of gammaherpesvirus
528 latency. *Nat Rev Microbiol*, **11**, 863-875.
529 9. Zhou, F., Shimoda, M., Olney, L., Lyu, Y., Tran, K., Jiang, G., Nakano, K., Davis, R.R.,
530 Tepper, C.G., Maverakis, E. *et al.* (2017) Oncolytic Reactivation of KSHV as a
531 Therapeutic Approach for Primary Effusion Lymphoma. *Mol Cancer Ther*, **16**, 2627-
532 2638.
533 10. Park, A., Oh, S., Jung, K.L., Choi, U.Y., Lee, H.R., Rosenfeld, M.G. and Jung, J.U.
534 (2020) Global epigenomic analysis of KSHV-infected primary effusion lymphoma
535 identifies functional MYC superenhancers and enhancer RNAs. *Proc Natl Acad Sci U S*
536 *A*, **117**, 21618-21627.
537 11. Gunther, T. and Grundhoff, A. (2010) The epigenetic landscape of latent Kaposi
538 sarcoma-associated herpesvirus genomes. *PLoS Pathog*, **6**, e1000935.
539 12. Maruo, S., Zhao, B., Johannsen, E., Kieff, E., Zou, J. and Takada, K. (2011) Epstein-Barr
540 virus nuclear antigens 3C and 3A maintain lymphoblastoid cell growth by repressing
541 p16INK4A and p14ARF expression. *Proc Natl Acad Sci U S A*, **108**, 1919-1924.
542 13. Murata, T., Kondo, Y., Sugimoto, A., Kawashima, D., Saito, S., Isomura, H., Kanda, T.
543 and Tsurumi, T. (2012) Epigenetic histone modification of Epstein-Barr virus BZLF1
544 promoter during latency and reactivation in Raji cells. *J Virol*, **86**, 4752-4761.
545 14. Gray, Z.H., Honer, M.A., Ghatalia, P., Shi, Y. and Whetstine, J.R. (2025) 20 years of
546 histone lysine demethylases: From discovery to the clinic and beyond. *Cell*, **188**, 1747-
547 1783.
548 15. Yoo, J., Kim, G.W., Jeon, Y.H., Kim, J.Y., Lee, S.W. and Kwon, S.H. (2022) Drawing a
549 line between histone demethylase KDM5A and KDM5B: their roles in development and
550 tumorigenesis. *Exp Mol Med*, **54**, 2107-2117.
551 16. Huang, H., Kong, W., Jean, M., Fiches, G., Zhou, D., Hayashi, T., Que, J., Santoso, N.
552 and Zhu, J. (2019) A CRISPR/Cas9 screen identifies the histone demethylase MINA53 as
553 a novel HIV-1 latency-promoting gene (LPG). *Nucleic Acids Res*, **47**, 7333-7347.

554 17. Gabaev, I., Williamson, J.C., Crozier, T.W.M., Schulz, T.F. and Lehner, P.J. (2020)
555 Quantitative Proteomics Analysis of Lytic KSHV Infection in Human Endothelial Cells
556 Reveals Targets of Viral Immune Modulation. *Cell Rep*, **33**, 108249.
557 18. Li, T.W., Park, Y., Watters, E.G., Wang, X., Zhou, D., Fiches, G.N., Wu, Z., Badley,
558 A.D., Sacha, J.B., Ho, W.Z. *et al.* (2024) KDM5A/B contribute to HIV-1 latent infection
559 and survival of HIV-1 infected cells. *Antiviral Res*, **228**, 105947.
560 19. Yu, Y., Wang, S.E. and Hayward, G.S. (2005) The KSHV immediate-early transcription
561 factor RTA encodes ubiquitin E3 ligase activity that targets IRF7 for proteosome-
562 mediated degradation. *Immunity*, **22**, 59-70.
563 20. Combs, L.R., Spires, L.M., Alonso, J.D., Papp, B. and Toth, Z. (2022) KSHV RTA
564 Induces Degradation of the Host Transcription Repressor ID2 To Promote the Viral Lytic
565 Cycle. *J Virol*, **96**, e0010122.
566 21. Kedes, D.H., Lagunoff, M., Renne, R. and Ganem, D. (1997) Identification of the gene
567 encoding the major latency-associated nuclear antigen of the Kaposi's sarcoma-associated
568 herpesvirus. *J Clin Invest*, **100**, 2606-2610.
569 22. Mercier, A., Arias, C., Madrid, A.S., Holdorf, M.M. and Ganem, D. (2014) Site-specific
570 association with host and viral chromatin by Kaposi's sarcoma-associated herpesvirus
571 LANA and its reversal during lytic reactivation. *J Virol*, **88**, 6762-6777.
572 23. Lan, K., Kuppers, D.A., Verma, S.C. and Robertson, E.S. (2004) Kaposi's sarcoma-
573 associated herpesvirus-encoded latency-associated nuclear antigen inhibits lytic
574 replication by targeting Rta: a potential mechanism for virus-mediated control of latency.
575 *J Virol*, **78**, 6585-6594.
576 24. Hu, J., Yang, Y., Turner, P.C., Jain, V., McIntyre, L.M. and Renne, R. (2014) LANA
577 binds to multiple active viral and cellular promoters and associates with the
578 H3K4methyltransferase hSET1 complex. *PLoS Pathog*, **10**, e1004240.
579 25. Toth, Z., Papp, B., Brulois, K., Choi, Y.J., Gao, S.J. and Jung, J.U. (2016) LANA-
580 Mediated Recruitment of Host Polycomb Repressive Complexes onto the KSHV Genome
581 during De Novo Infection. *PLoS Pathog*, **12**, e1005878.
582 26. Zhang, G., Chan, B., Samarina, N., Abere, B., Weidner-Glunde, M., Buch, A., Pich, A.,
583 Brinkmann, M.M. and Schulz, T.F. (2016) Cytoplasmic isoforms of Kaposi sarcoma
584 herpesvirus LANA recruit and antagonize the innate immune DNA sensor cGAS. *Proc*
585 *Natl Acad Sci U S A*, **113**, E1034-1043.
586 27. Mariggio, G., Koch, S., Zhang, G., Weidner-Glunde, M., Ruckert, J., Kati, S., Santag, S.
587 and Schulz, T.F. (2017) Kaposi Sarcoma Herpesvirus (KSHV) Latency-Associated
588 Nuclear Antigen (LANA) recruits components of the MRN (Mre11-Rad50-NBS1) repair
589 complex to modulate an innate immune signaling pathway and viral latency. *PLoS*
590 *Pathog*, **13**, e1006335.
591 28. Cloutier, N. and Flamand, L. (2010) Kaposi sarcoma-associated herpesvirus latency-
592 associated nuclear antigen inhibits interferon (IFN) beta expression by competing with
593 IFN regulatory factor-3 for binding to IFNB promoter. *J Biol Chem*, **285**, 7208-7221.
594 29. Johansson, C., Velupillai, S., Tumber, A., Szykowska, A., Hookway, E.S., Nowak, R.P.,
595 Strain-Damerell, C., Gileadi, C., Philpott, M., Burgess-Brown, N. *et al.* (2016) Structural
596 analysis of human KDM5B guides histone demethylase inhibitor development. *Nat Chem*
597 *Biol*, **12**, 539-545.

598 30. Ohguchi, H., Park, P.M.C., Wang, T., Gryder, B.E., Ogiya, D., Kurata, K., Zhang, X., Li,
599 D., Pei, C., Masuda, T. *et al.* (2021) Lysine Demethylase 5A is Required for MYC
600 Driven Transcription in Multiple Myeloma. *Blood Cancer Discov*, **2**, 370-387.
601 31. Pidugu, V.K., Wu, M.M., Yen, A.H., Pidugu, H.B., Chang, K.W., Liu, C.J. and Lee, T.C.
602 (2019) IFIT1 and IFIT3 promote oral squamous cell carcinoma metastasis and contribute
603 to the anti-tumor effect of gefitinib via enhancing p-EGFR recycling. *Oncogene*, **38**,
604 3232-3247.
605 32. Botti, E., Spallone, G., Moretti, F., Marinari, B., Pinetti, V., Galanti, S., De Meo, P.D.,
606 De Nicola, F., Ganci, F., Castrignano, T. *et al.* (2011) Developmental factor IRF6
607 exhibits tumor suppressor activity in squamous cell carcinomas. *Proc Natl Acad Sci U S*
608 *A*, **108**, 13710-13715.
609 33. Boehmer, D.F.R., Formisano, S., de Oliveira Mann, C.C., Mueller, S.A., Kluge, M.,
610 Metzger, P., Rohlfs, M., Horth, C., Kocheise, L., Lichtenthaler, S.F. *et al.* (2021)
611 OAS1/RNase L executes RIG-I ligand-dependent tumor cell apoptosis. *Sci Immunol*, **6**.
612 34. Speck, S.H. and Ganem, D. (2010) Viral latency and its regulation: lessons from the
613 gamma-herpesviruses. *Cell Host Microbe*, **8**, 100-115.
614 35. Damania, B. (2004) Oncogenic gamma-herpesviruses: comparison of viral proteins
615 involved in tumorigenesis. *Nat Rev Microbiol*, **2**, 656-668.
616 36. Rasmussen, P.B. and Staller, P. (2014) The KDM5 family of histone demethylases as
617 targets in oncology drug discovery. *Epigenomics*, **6**, 277-286.
618 37. Hou, J., Wu, J., Dombkowski, A., Zhang, K., Holowatyj, A., Boerner, J.L. and Yang, Z.Q.
619 (2012) Genomic amplification and a role in drug-resistance for the KDM5A histone
620 demethylase in breast cancer. *Am J Transl Res*, **4**, 247-256.
621 38. Yamamoto, S., Wu, Z., Russnes, H.G., Takagi, S., Peluffo, G., Vaske, C., Zhao, X.,
622 Moen Vollan, H.K., Maruyama, R., Ekram, M.B. *et al.* (2014) JARID1B is a luminal
623 lineage-driving oncogene in breast cancer. *Cancer Cell*, **25**, 762-777.
624 39. Hinohara, K., Wu, H.J., Vigneau, S., McDonald, T.O., Igarashi, K.J., Yamamoto, K.N.,
625 Madsen, T., Fassl, A., Egri, S.B., Papanastasiou, M. *et al.* (2018) KDM5 Histone
626 Demethylase Activity Links Cellular Transcriptomic Heterogeneity to Therapeutic
627 Resistance. *Cancer Cell*, **34**, 939-953 e939.
628 40. Yamane, K., Tateishi, K., Klose, R.J., Fang, J., Fabrizio, L.A., Erdjument-Bromage, H.,
629 Taylor-Papadimitriou, J., Tempst, P. and Zhang, Y. (2007) PLU-1 is an H3K4
630 demethylase involved in transcriptional repression and breast cancer cell proliferation.
631 *Mol Cell*, **25**, 801-812.
632 41. Zeng, J., Ge, Z., Wang, L., Li, Q., Wang, N., Bjorkholm, M., Jia, J. and Xu, D. (2010)
633 The histone demethylase RBP2 Is overexpressed in gastric cancer and its inhibition
634 triggers senescence of cancer cells. *Gastroenterology*, **138**, 981-992.
635 42. Li, Y., Chen, L., Feng, L., Zhu, M., Shen, Q., Fang, Y., Liu, X. and Zhang, X. (2019)
636 NEK2 promotes proliferation, migration and tumor growth of gastric cancer cells via
637 regulating KDM5B/H3K4me3. *Am J Cancer Res*, **9**, 2364-2378.
638 43. Li, H., Wawrose, J.S., Gooding, W.E., Garraway, L.A., Lui, V.W., Peyser, N.D. and
639 Grandis, J.R. (2014) Genomic analysis of head and neck squamous cell carcinoma cell
640 lines and human tumors: a rational approach to preclinical model selection. *Mol Cancer*
641 *Res*, **12**, 571-582.

642 44. Huang, D., Qiu, Y., Li, G., Liu, C., She, L., Zhang, D., Chen, X., Zhu, G., Zhang, X.,
643 Tian, Y. *et al.* (2018) KDM5B overexpression predicts a poor prognosis in patients with
644 squamous cell carcinoma of the head and neck. *J Cancer*, **9**, 198-204.
645 45. Oser, M.G., Sabet, A.H., Gao, W., Chakraborty, A.A., Schinzel, A.C., Jennings, R.B.,
646 Fonseca, R., Bonal, D.M., Booker, M.A., Flaifel, A. *et al.* (2019) The KDM5A/RBP2
647 histone demethylase represses NOTCH signaling to sustain neuroendocrine
648 differentiation and promote small cell lung cancer tumorigenesis. *Genes Dev*, **33**, 1718-
649 1738.
650 46. Kuo, K.T., Huang, W.C., Bamodu, O.A., Lee, W.H., Wang, C.H., Hsiao, M., Wang, L.S.
651 and Yeh, C.T. (2018) Histone demethylase JARID1B/KDM5B promotes aggressiveness
652 of non-small cell lung cancer and serves as a good prognostic predictor. *Clin Epigenetics*,
653 **10**, 107.
654 47. Heward, J., Konali, L., D'Avola, A., Close, K., Yeomans, A., Philpott, M., Dunford, J.,
655 Rahim, T., Al Seraihi, A.F., Wang, J. *et al.* (2021) KDM5 inhibition offers a novel
656 therapeutic strategy for the treatment of KMT2D mutant lymphomas. *Blood*, **138**, 370-
657 381.
658 48. Xu, D., Bewicke-Copley, F., Close, K., Okosun, J., Gale, R.P., Apperley, J., Weinstock,
659 D.M., Wendel, H.G. and Fitzgibbon, J. (2024) Targeting lysine demethylase 5 (KDM5)
660 in mantle cell lymphoma. *Blood Cancer J*, **14**, 29.
661 49. Vallianatos, C.N., Farrehi, C., Friez, M.J., Burmeister, M., Keegan, C.E. and Iwase, S.
662 (2018) Altered Gene-Regulatory Function of KDM5C by a Novel Mutation Associated
663 With Autism and Intellectual Disability. *Front Mol Neurosci*, **11**, 104.
664 50. Li, J., Lan, Z., Liao, W., Horner, J.W., Xu, X., Liu, J., Yoshihama, Y., Jiang, S., Shim,
665 H.S., Slotnik, M. *et al.* (2023) Histone demethylase KDM5D upregulation drives sex
666 differences in colon cancer. *Nature*, **619**, 632-639.
667 51. Scandaglia, M., Lopez-Atalaya, J.P., Medrano-Fernandez, A., Lopez-Cascales, M.T., Del
668 Blanco, B., Lipinski, M., Benito, E., Olivares, R., Iwase, S., Shi, Y. *et al.* (2017) Loss of
669 Kdm5c Causes Spurious Transcription and Prevents the Fine-Tuning of Activity-
670 Regulated Enhancers in Neurons. *Cell Rep*, **21**, 47-59.
671 52. Munz, C. (2021) The Role of Lytic Infection for Lymphomagenesis of Human gamma-
672 Herpesviruses. *Front Cell Infect Microbiol*, **11**, 605258.
673 53. Lurain, K., Ramaswami, R., Oksenhendler, E., Boutboul, D., Dalla Pria, A., Ulrich, L.,
674 Shanmugasundaram, K., Uldrick, T.S., Bower, M., Yarchoan, R. *et al.* (2025) Primary
675 Effusion Lymphoma Prognostic Score (PEL-PS): A Validated International Prognostic
676 Score in HIV-Associated Primary Effusion Lymphoma. *Am J Hematol*, **100**, 393-401.
677 54. Fiches, G.N., Wu, Z., Zhou, D., Biswas, A., Li, T.W., Kong, W., Jean, M., Santoso, N.G.
678 and Zhu, J. (2022) Polyamine biosynthesis and eIF5A hypusination are modulated by the
679 DNA tumor virus KSHV and promote KSHV viral infection. *PLoS Pathog*, **18**, e1010503.
680 55. Zhou, D., Hayashi, T., Jean, M., Kong, W., Fiches, G., Biswas, A., Liu, S., Yosief, H.O.,
681 Zhang, X., Bradner, J. *et al.* (2020) Inhibition of Polo-like kinase 1 (PLK1) facilitates the
682 elimination of HIV-1 viral reservoirs in CD4(+) T cells ex vivo. *Sci Adv*, **6**, eaba1941.
683 56. Biswas, A., Zhou, D., Fiches, G.N., Wu, Z., Liu, X., Ma, Q., Zhao, W., Zhu, J. and
684 Santoso, N.G. (2021) Inhibition of polo-like kinase 1 (PLK1) facilitates reactivation of
685 gamma-herpesviruses and their elimination. *PLoS Pathog*, **17**, e1009764.
686 57. Zhou, D., Wu, Z., Park, J.G., Fiches, G.N., Li, T.W., Ma, Q., Huang, H., Biswas, A.,
687 Martinez-Sobrido, L., Santoso, N.G. *et al.* (2022) FACT subunit SUPT16H associates

688 with BRD4 and contributes to silencing of interferon signaling. *Nucleic Acids Res*, **50**,
689 8700-8718.
690 58. Love, M.I., Huber, W. and Anders, S. (2014) Moderated estimation of fold change and
691 dispersion for RNA-seq data with DESeq2. *Genome Biol*, **15**, 550.
692

693

694 **Figures**

695 **Figure 1.** KSHV lytic program targets KDM5A/B for proteasome degradation. (A)
696 TREx.BCBL-1.RTA cells were treated with doxycycline (Dox, 1 μg/mL) for 2 days, followed by
697 protein immunoblotting to quantify KDM5A/B proteins and KSHV lytic K8.1 protein. (B)
698 KDM5A/B mRNA level in cell samples (A) was measured by RT-qPCR. (C) BJAB cells were
699 treated similarly as (A) and analyzed by protein immunoblotting to quantify KDM5A/B proteins.
700 (D) KDM5A/B mRNA level in cell samples (C) was measured by RT-qPCR. (E) TIME cells
701 were spinoculated with KSHV BAC16 viruses. At 2 days post of infection (dpi), cells were
702 collected and analyzed by protein immunoblotting to quantify KDM5A/B proteins and KSHV
703 lytic K8.1 protein. (F) KDM5A/B mRNA level in cell samples (E) was measured by RT-qPCR.
704 (G) TREx.BCBL-1.RTA cells were treated with Dox in the absence or presence of MG132 (1
705 μM) for 2 days, followed by protein immunoblotting to quantify KDM5A/B proteins and KSHV
706 lytic K8.1 protein. (H, I) TREx.BCBL-1.RTA cells were treated with Dox in the absence or
707 presence of MG132 (1 μM) for 2 days, followed by protein immunoprecipitation (IP) of
708 KDM5A (H) or KDM5B (I) using their specific antibodies, followed by protein immunoblotting
709 to quantify K48 or K63-linked polyubiquitination of KDM5A/B. Results were calculated from
710 three independent experiments and presented as Mean ± SD (ns: not significant, * $P < 0.05$, ** P
711 < 0.01, **** $P < 0.0001$; unpaired, two-tailed Student's *t*-test).

712

713 **Figure 2.** KDM5A/B suppress KSHV lytic reactivation from latency. (A, B) TREx.BCBL-
714 1.RTA cells were transiently transfected with siRNAs targeting KDM5A (A) or KDM5B (B)
715 through electroporation. At 3 days post of transfection, cells were collected and analyzed by RT-
716 qPCR to quantify KDM5A/B knockdown. (C, D) TREx.BCBL-1.RTA cells with depletion of

717 KDM5A (C) or KDM5B (D) were treated with Dox for 2 days, followed by RT-qPCR to
718 quantify KSHV lytic genes K8 and K8.1. (E, F) KDM5A/B and KSHV K8.1 proteins in cell
719 samples (C, D) with Dox treatment were measured by protein immunoblotting. (G, H)
720 iSLK.BAC16 cells were transiently transfected with siRNAs targeting KDM5A (G) or KDM5B
721 (H) for 3 days, followed by Dox treatment for 2 days. KDM5A/B knockdown were measured by
722 RT-qPCR. (I, J) iSLK.BAC16 cells with depletion of KDM5A (I) or KDM5B (J) as well as Dox
723 treatment was analyzed by RT-qPCR to quantify KSHV lytic genes K8 and K8.1. (K, L)
724 KDM5A/B and KSHV K8.1 proteins in cell samples in cell samples (I, J) were measured by
725 protein immunoblotting. (M, N) iSLK.r219 cells were transiently transfected with siRNAs
726 targeting KDM5A (M) or KDM5B (N) for 3 days, followed by Dox treatment for 2 days.
727 KDM5A/B knockdown were measured by RT-qPCR. KSHV lytic reactivation was visualized by
728 fluorescence microscopy (RFP *vs* GFP signal). Results were calculated from three independent
729 experiments and presented as Mean ± SD (*** $P < 0.001$, **** $P < 0.0001$; unpaired, two-tailed
730 Student's *t*-test for A; one-way ANOVA for I, J, two-way ANOVA for B, C, E, F, G).
731
732 **Figure 3.** KDM5A/B associate with KSHV LANA and modulate its functions. (A, B)
733 Average profile plot (A) and heatmap (B) showing the ChIP-seq enrichment pattern of RNAP1,
734 LANA (KSHV), RTA (KSHV), and H3K4me3 at promoter regions of immune-responsive genes
735 (IRGs) were presented, which were generated from re-analysis of the public ChIP-seq dataset
736 (GSE202670). (C, D) BCBL-1 (C) or iSLK.BAC16 (D) cells were collected for protein IP of
737 KSHV LANA, followed by protein immunoblotting to quantify the co-IPed KDM5A/B protein.
738 (E, F) iSLK.BAC16 cells were subjected to protein immunofluorescence followed by confocal
739 microscopy imaging to visualize the co-localization of KSHV LANA protein with KDM5A (E)

740 or KDM5B (F). (G, H) iSLK.BAC16 cells were transiently transfected with siRNAs targeting
741 KDM5A/B for 3 days. Cells were collected for chromatin immunoprecipitation (ChIP) of KSHV
742 LANA protein using its antibody or the control rat IgG, followed by qPCR to quantify the
743 binding of LANA at the promoter regions of KSHV RTA (G) or host IRGs (H). Results were
744 calculated from three independent experiments and presented as Mean ± SD (**** $P < 0.0001$;
745 two-way ANOVA).
746
747 **Figure 4.** KDM5 inhibition induces KSHV lytic reactivation from latency. (A) TREx.BCBL-
748 1.RTA cells treated with JQKD82 (48 h) was analyzed by the ATP luminescent assay to measure
749 drug's cytotoxicity. (B) TREx.BCBL-1.RTA cells were treated with JQKD82 for 48 h and then
750 Dox for another 48 h. Cells were collected for protein immunoblotting of KSHV lytic K8.1
751 protein. (C) mRNA level of KSHV lytic viral genes (ORF50/RTA, K8, K8.1) in cell samples (B)
752 was measured by RT-qPCR. (D, E) BCBL-1 (D) or BC-3 cells (E) were treated with JQKD82 for
753 96 h and analyzed by RT-qPCR to quantify KSHV lytic genes K8 and K8.1. (F) iSLK.BAC16
754 cells were treated with JQKD82 for 48 h and then Dox for another 48 h. Cells were collected for
755 protein immunoblotting to quantify KSHV K8.1 protein. (G) iSLK.BAC16 cells treated with
756 JQKD82 in the absence or presence of Dox were collected and analyzed by RT-qPCR to
757 quantify KSHV lytic genes K8 and K8.1. Results were calculated from three independent
758 experiments and presented as Mean ± SD (** $P < 0.01$, *** $P < 0.001$, **** $P < 0.0001$;
759 unpaired, two-tailed Student's *t*-test for D, E; two-way ANOVA for C, G).
760
761 **Figure 5.** KDM5 inhibition induces antiviral/antitumor innate immune responses. (A, B)
762 BCBL-1 (A) and BJAB (B) cells were treated with JQKD82 (20 μM) for 4 days, followed by

763 RNA-seq analysis. A volcano plot was used to profile the differential gene expression induced
764 by JQKD82 treatment. Several upregulated antiviral/antitumor IRGs were highlighted. (C) GO
765 analysis was performed by using g:Profiler to identify the pathway enrichment for JQKD82-
766 treated BCBL-1 cells . Several immune-related pathways were highlighted. (D) Heatmap was
767 plotted for the selected differentially expressed antiviral/antitumor IRGs in JQKD82-treated
768 BCBL-1 cells. (E-G) BCBL-1 cells were treated with JQKD82 (20 μM) for 4 days, followed by
769 RT-qPCR to quantify the expression of IRGs shared with both JQKD82-treated BCBL-1 and
770 BJAB cells (E), KSHV K8 (F), and IRGs only upregulated in JQKD82-treated BCBL-1 cells (G).
771 Results were calculated from three independent experiments and presented as Mean ± SD (* $P <$
772 0.05, ** $P < 0.01$, *** $P < 0.001$, **** $P < 0.0001$; unpaired, two-tailed Student's *t*-test).
773
774 **Figure 6.** KDM5 inhibition promotes the death of KSHV-positive PEL cells *in vitro*. (A)
775 BJAB and primary B cells (3 heathy donors) were collected and analyzed by protein
776 immunoblotting to quantify KDM5A/B proteins. (B) KSHV-positive (BCBL-1, BC-3) and
777 KSHV-negative (BJAB, Ramos) B-cell lymphoma lines were collected and analyzed by protein
778 immunoblotting to quantify KDM5A/B proteins. (C, D) De-identified lymph node tissue samples
779 (2 healthy donors, 2 diffuse large B-cell lymphoma [DLBCL] patients) were collected and
780 analyzed by protein immunofluorescence to visualize KDM5A (C) or KDM5B (D) protein
781 (Alexa Fluor 647). B-cell marker CD20 was also immuno-stained (Alexa Fluor 488). (E) BJAB
782 and primary B cells (3 heathy donors) were treated with JQKD82 (20 μM) up to 5 days and
783 analyzed by the ATP-based cell viability assay at each day. (F, G) BCBL-1 (F) or BC-3 (G) cells
784 along with BJAB cells were treated with JQKD82 (20 μM) up to 5 days and analyzed by the cell

785 viability assay at each day. Results were calculated from three independent experiments and
786 presented as Mean ± SD (** $P < 0.01$, **** $P < 0.0001$; unpaired, two-tailed Student's *t*-test).
787
788 **Figure 7.** KDM5 inhibition blocks the tumor growth of KSHV-positive PEL cells *in vivo*. (A)
789 A PEL xenograft mouse model was used to evaluate the anti-tumor effect of KDM5 inhibition.
790 Briefly, NSG mice were intraperitoneally (i.p.) transplanted with BCBL-1-Luc cells. At one
791 week post of transplantation, mice were randomized to receive vehicle or JQKD82 that was
792 administrated i.p. at 50 mg/kg every two days for two weeks. Tumor growth was monitored by
793 bioluminescence imaging (BLI) by using the IVIS Spectrum 2 system twice a week for three
794 weeks. (B) Representative images of PEL tumors in either vehicle or JQKD82 mouse group at 28
795 days post of transplantation were illustrated. (C) Fluc activity (total flux) indicating tumor
796 burden was plotted up to 28 days post of transplantation. (D) Mice were euthanized at Day 29.
797 Tumors were collected from either vehicle or JQKD82 mouse group and photographed for
798 visualization. (E-G) Ascites from tumor sites were also collected from the euthanized mice.
799 Tumor volume (E), tumor weight (F), and ascites volume (G) were measured and compared
800 between vehicle and JQKD82 mouse groups. (H, I) Total RNAs were extracted from harvested
801 tumor samples and analyzed by RT-qPCR to quantify the mRNA level of KSHV viral genes (H)
802 or antitumor IRGs (I). Results were calculated from 4 mice of each condition and presented as
803 either Mean ± SD (for C) or Mean ± SEM (for E, F, G, H, I) (* $P < 0.05$, ** $P < 0.01$, *** $P <$
804 0.001, **** $P < 0.0001$; unpaired, two-tailed Student's *t*-test for C; unpaired, one-tailed Student's
805 *t*-test for E, F, G, H, I).
806
807

808 **Figure 1**

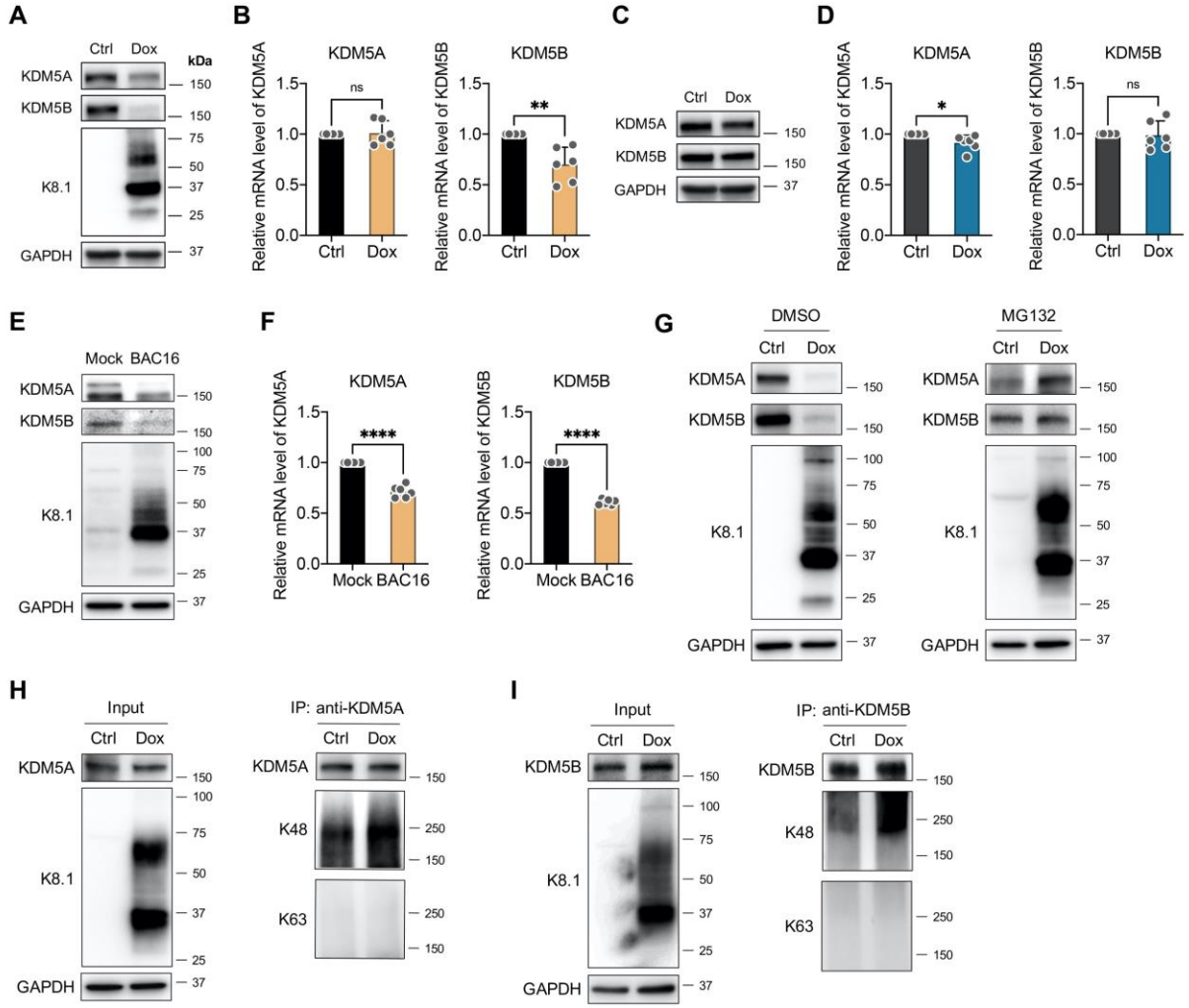

809

810

811

Figure 2

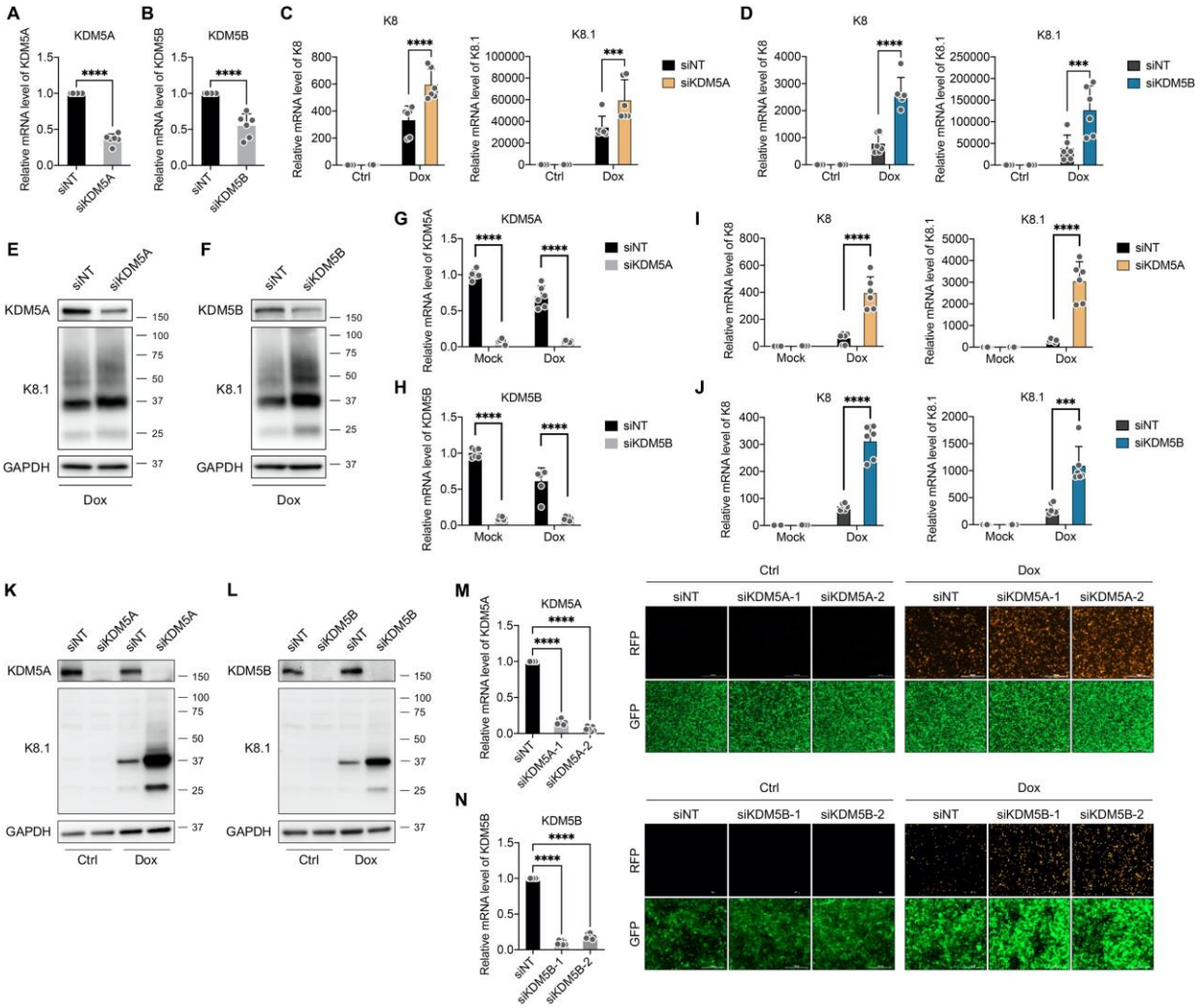
A
KDM5A
Relative mRNA level of KDM5A
siNT
siKDM5A
B
KDM5B
Relative mRNA level of KDM5B
siNT
siKDM5B
C
K8
K8.1
Relative mRNA level of K8
Relative mRNA level of K8.1
Ctrl
Dox
siNT
siKDM5A
D
K8
K8.1
Relative mRNA level of K8
Relative mRNA level of K8.1
Ctrl
Dox
siNT
siKDM5B
E
siNT
siKDM5A
KDM5A
K8.1
GAPDH
Dox
F
siNT
siKDM5B
KDM5B
K8.1
GAPDH
Dox
G
KDM5A
Relative mRNA level of KDM5A
Mock
Dox
siNT
siKDM5A
H
KDM5B
Relative mRNA level of KDM5B
Mock
Dox
siNT
siKDM5B
I
K8
K8.1
Relative mRNA level of K8
Relative mRNA level of K8.1
Mock
Dox
siNT
siKDM5A
J
K8
K8.1
Relative mRNA level of K8
Relative mRNA level of K8.1
Mock
Dox
siNT
siKDM5B
K
siNT
siKDM5A
siNT
siKDM5A
KDM5A
K8.1
GAPDH
Ctrl
Dox
L
siNT
siKDM5B
siNT
siKDM5B
KDM5B
K8.1
GAPDH
Ctrl
Dox
M
KDM5A
Relative mRNA level of KDM5A
siNT
siKDM5A-1
siKDM5A-2
Ctrl
Dox
siNT
siKDM5A-1
siKDM5A-2
RFP
GFP
N
KDM5B
Relative mRNA level of KDM5B
siNT
siKDM5B-1
siKDM5B-2
Ctrl
Dox
siNT
siKDM5B-1
siKDM5B-2
RFP
GFP

816 **Figure 3**

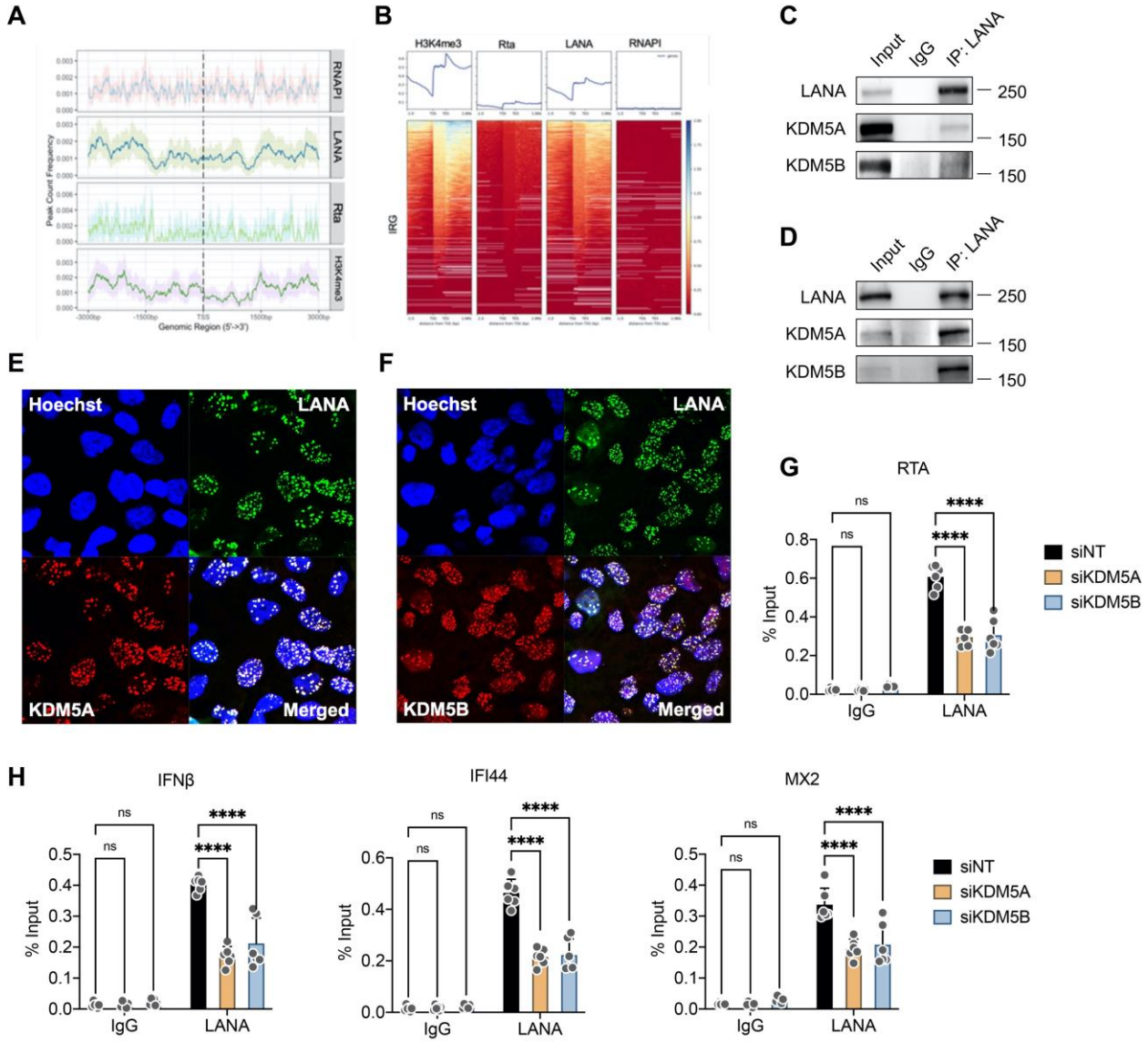

817

818

819

820 **Figure 4**

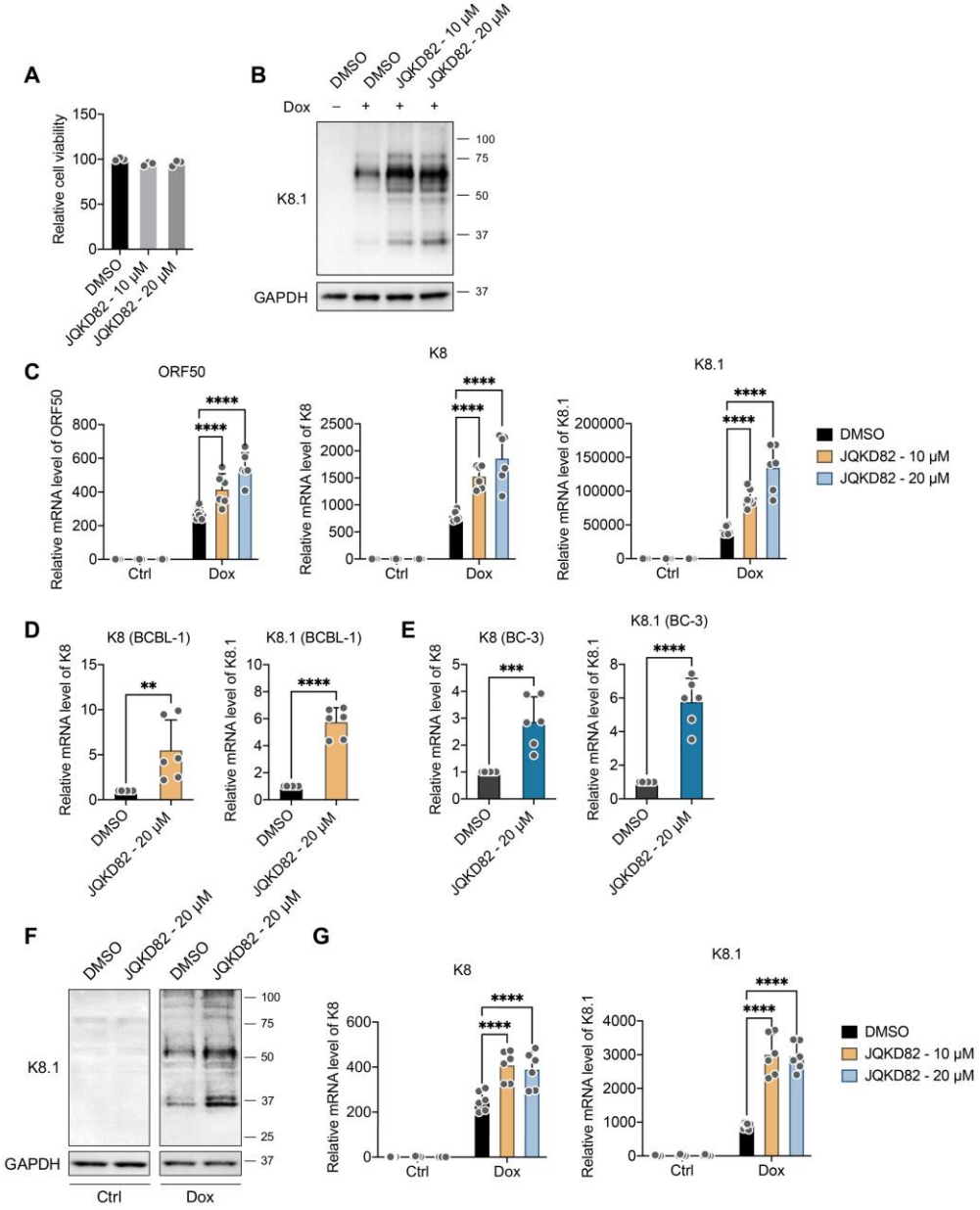

821

822

823

824 **Figure 5**

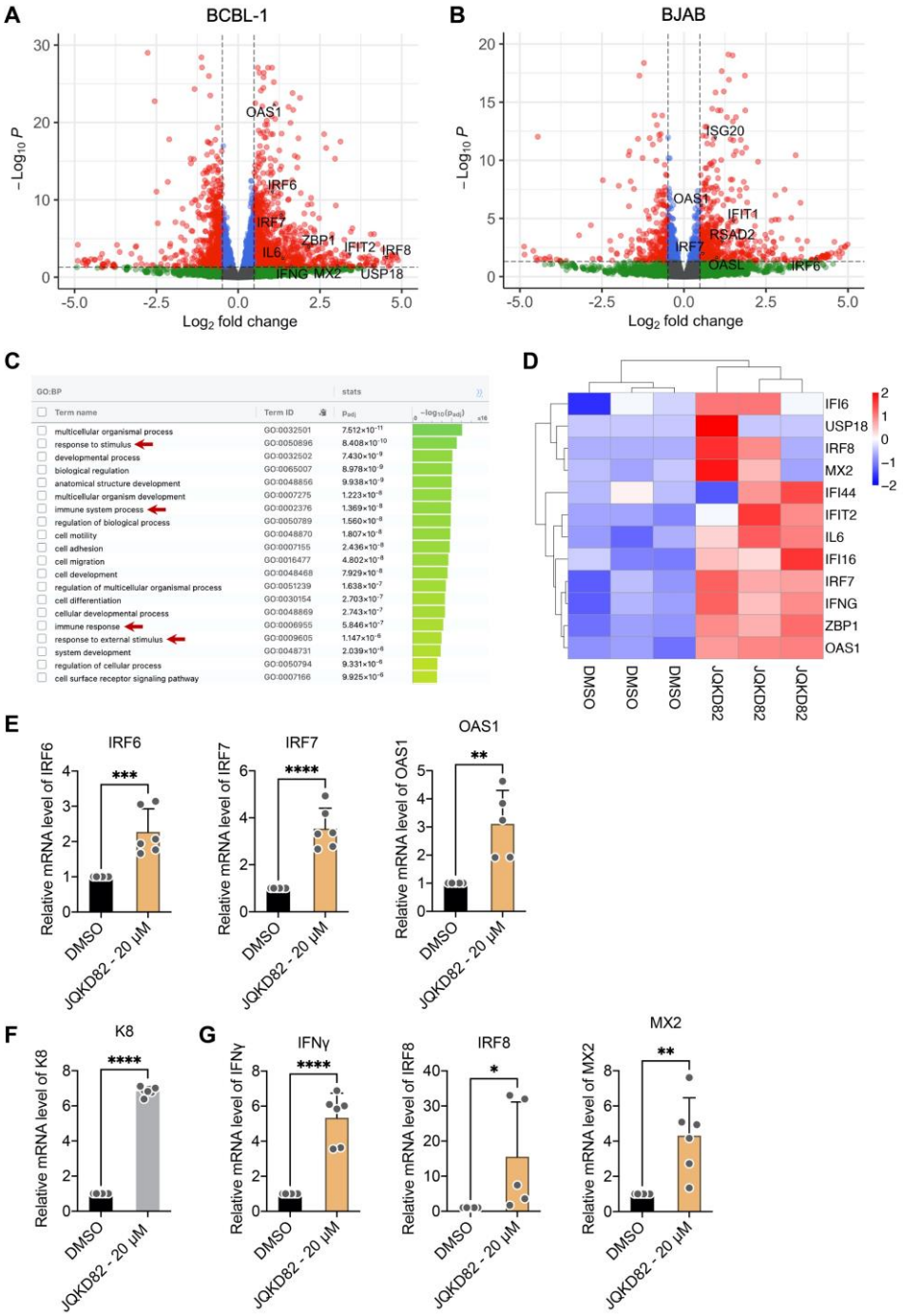

825

826

827

Figure 6

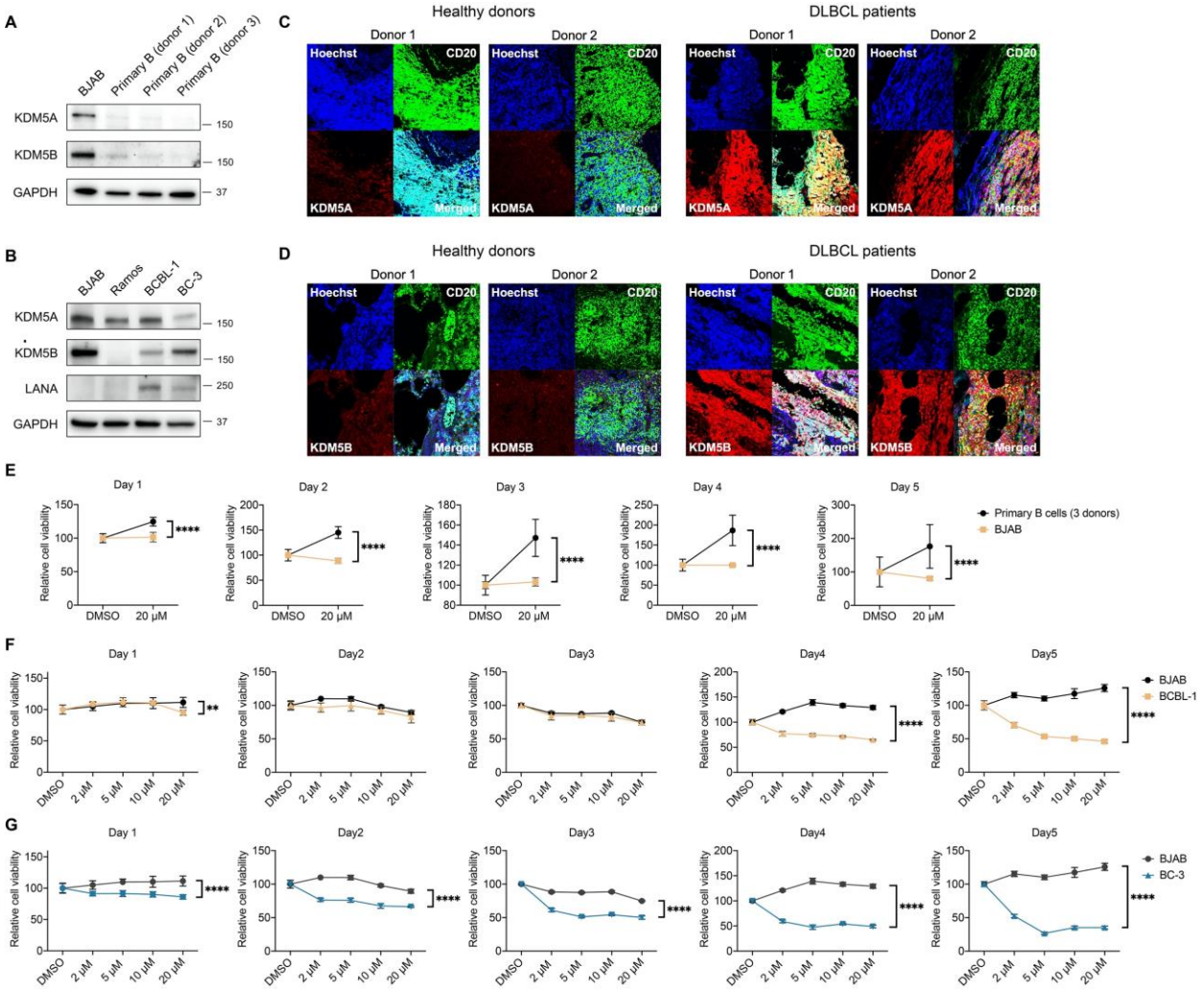
A
BJAB
Primary B (donor 1)
Primary B (donor 2)
Primary B (donor 3)
KDM5A
KDM5B
GAPDH
150
150
37
B
BJAB
Ramos
BCBL-1
BC-3
KDM5A
KDM5B
LANA
GAPDH
150
150
250
37
C
Healthy donors
DLBCL patients
Donor 1
Donor 2
Hoechst
CD20
KDM5A
Merged
D
KDM5B
E
Day 1
Day 2
Day 3
Day 4
Day 5
Relative cell viability
DMSO
20 μM
****
Primary B cells (3 donors)
BJAB
F
Day1
Day2
Day3
Day4
Day5
2 μM
5 μM
10 μM
20 μM
**
BCBL-1
G
BC-3

832 **Figure 7**

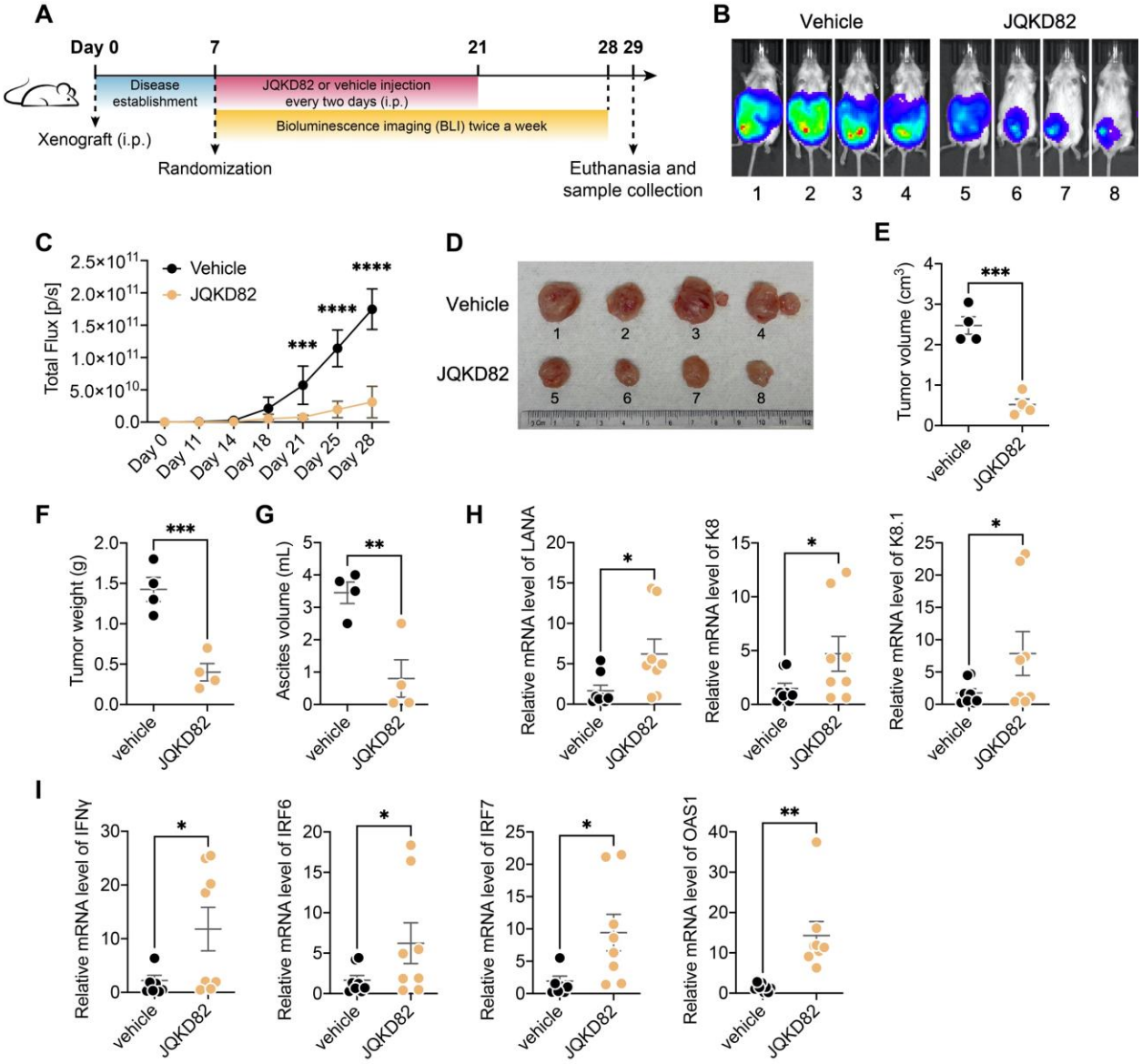

833

834

835